Phase-mediated long-range interactions of cavity solitons in a semiconductor laser with a saturable absorber

H. Vahed,[1] R. Kheradmand,[2] H. Tajalli,[1,2] G. Tissoni,[3,5] L. A. Lugiato,[4,5] and F. Prati[4,5]

[1]*Faculty of Physics, University of Tabriz, Tabriz, Iran*

[2]*Photonics Group, Research Institute for Applied Physics and Astronomy, University of Tabriz, Tabriz, Iran*

[3]*Institut Non Linéaire de Nice, CNRS, Université de Nice Sophia Antipolis, UMR 6618, 1361 Route des Lucioles, F-06560 Valbonne, France*

[4]*Dipartimento di Fisica e Matematica, Università dell'Insubria, Via Valleggio 11, I-22100 Como, Italy*

[5]*CNISM, Research Unit of Como, Via Valleggio 11, I-22100 Como, Italy*

(Received 29 September 2011; published 5 December 2011)

We numerically study the dynamics of pairs of cavity solitons in a laser. We show that the solitons interact even at distances much greater than their sizes in the intensity and carrier-densities profile. The interaction is mediated by the phase. In a certain range of initial values of the distance, the solitons adjust their position until they form bound states. There are two such bound states, corresponding to different equilibrium distances, in which the solitons display partial phase locking, that is, their relative phase slowly oscillates as in a phase-entrained state. In those states, the two solitons can be switched on and off independently. For smaller initial distances, only one soliton survives. For larger initial distances, the solitons lock in phase and repel each other up to a distance of about ten soliton diameters.

DOI: 10.1103/PhysRevA.84.063814 PACS number(s): 42.65.Tg, 42.65.Sf, 42.55.Px

I. INTRODUCTION

Recently, a new kind of laser has emerged from studies on cavity solitons (CSs): the CS laser (CSL) [1]. An intermediate step toward the realization of a CSL was the vertical-cavity surface-emitting laser (VCSEL) with optical injection where the CSs form through a mechanism that is essentially the same as in early experiments with passive devices or amplifiers [2]. The only relevant difference was that, in a VCSEL above threshold, optical injection can cause an instability in the lower branch of the bistable curve, and this produces a turbulent dynamics in the background of the solitons [3].

But the breakthrough was the demonstration that a CSL can be realized without the need of an external driving field. In this way, one has a laser that, although homogeneously pumped over its transverse section, emits isolated beams placed in arbitrary positions and surrounded by regions of pure spontaneous emission. Such a device can be regarded as an array of microlasers, which, compared to conventional arrays, presents several applicative advantages related to the fact that the positions of the single emitters are not fixed *a priori* and they even can move, spontaneously or not.

Two physical mechanisms make it possible to realize a CSL: frequency-selective feedback from a volume Bragg grating [4–6] and inclusion of a saturable absorber. In the latter case, two different experimental setups were adopted: two VCSELs, one above and the other below transparency, in a face-to-face configuration [7–9], and a monolithic cavity that contains both an amplifying and an absorbing stage [10,11].

The last configuration was studied extensively in a series of theoretical papers [12–15] based on model equations similar to those used by Rozanov and Fedorov [16] and Fedorov *et al.* [17], who, almost 20 yr ago, made the prediction for localized structures (autosolitons) in a laser with a saturable absorber. With respect to an externally driven system where the coherent holding beam locks the phases of all the CSs to the same value, in a CSL, the absence of a driving field introduces a new degree of freedom, the relative phase, in the interaction of CSs.

In driven systems, the CSs can merge, can repel until they reach a critical distance beyond which they do not interact anymore [18,19], and can form clusters at some equilibrium distances, which are the minima of an oscillating potential produced by the tails in their intensity profile [20]. The phase plays no role in these interactions.

In a CSL, instead, phase-dependent interactions may be expected, such as in spatial solitons [21], and the range of the interactions can be very large because, as we show, the phase profile of the CS has a size much larger than the intensity profile. It must be stressed, however, that in the case of propagating solitons the phases are determined by the launching conditions, while in a CSL, they are free dynamical variables.

In this respect, CSs in a CSL are more similar to (micro)lasers in an array, where each laser can choose its phase freely. It is known that semiconductor laser arrays manifest a preference for the out-of-phase state. Such a preference commonly is attributed to the fact that this state, where the field intensity exactly is zero in between two lasers, better matches the gain profile of etched arrays. Yet, the analysis of the dynamical equations shows that such a preference can also be attributed to the nonlinear dispersion induced by the linewidth enhancement factor [22,23], which favors the out-of-phase state because it is blue detuned with respect to the in-phase state. Accordingly, the out-of-phase state should be the preferred one in any array of semiconductor lasers, even in an array of CSs with a homogeneous gain profile, such as a CSL, at least, as long as the distance between the CSs is fixed.

Previous numerical analysis of the interaction of solitons in a laser with a saturable absorber in the limit of fast material dynamics showed that both in-phase [24] and out-of-phase [25] pairs of two-dimensional stationary solitons can be stable. When the finite-relaxation times of the material variables are taken into account, moving clusters of solitons are found [26]. However, with respect to those papers, in our model we

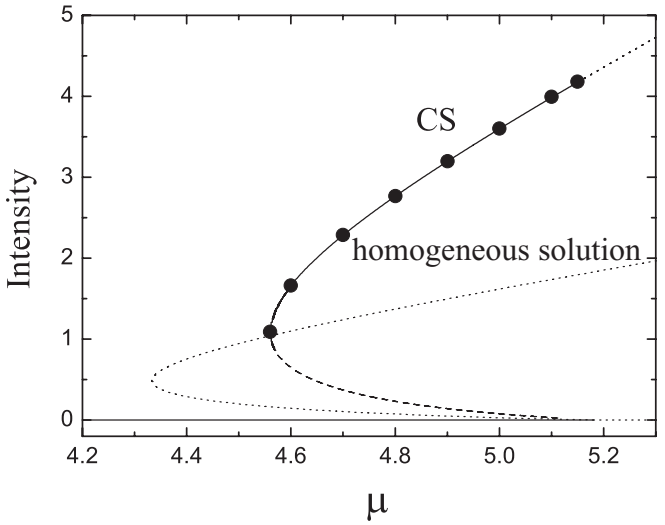

FIG. 1. Intensity of the homogeneous stationary states and of the CS for $s = 1$, $\gamma = 2$, $B = 0.1$, $\alpha = 2$, $\beta = 1$, and $b_1 = b_2 = 0.003$ as a function of the pump parameter μ. For the CS, the symbol represents the peak intensity of the stable solution.

include the linewidth enhancement factor, which, for what is mentioned above, is expected to play a relevant role.

In this paper, we study how the interaction of two CSs depends on their distance. We start from an initial condition where only one CS is present, and we switch on another one at progressively larger distances. We use incoherent switching because that is the technique adopted in the monolithic device [11]. After reviewing the model and its stationary solutions in Sec. II, in Sec. III, we classify the different behaviors observed at various distances. Section IV contains a summary of the results and a comparison with recent experimental findings.

II. DYNAMICAL EQUATIONS AND STATIONARY SOLUTIONS

The dynamics of a VCSEL-based CS laser is described by the following set of equations [13]:

$$\dot{F} = [(1 - i\alpha)D + (1 - i\beta)d - 1 + i\nabla^2]F, \quad (1)$$

$$\dot{D} = b_1[\mu - D(1 + |F|^2) - BD^2], \quad (2)$$

$$\dot{d} = b_2[-\gamma - d(1 + s|F|^2) - Bd^2]. \quad (3)$$

F is the slowly varying amplitude of the electric field, and D and d are population variables defined as

$$D = \eta_1 \left(\frac{N_1}{N_{1,0}} - 1 \right), \quad d = \eta_2 \left(\frac{N_2}{N_{2,0}} - 1 \right), \quad (4)$$

where N_1 and N_2 are the carrier densities in the active and passive materials, respectively, $N_{1,0}$ and $N_{2,0}$ are their transparency values, and η_1 and η_2 are adimensional coefficients related to gain and absorption, respectively.

The parameters α and b_1 (β and b_2) are the linewidth enhancement factor and the ratio of the photon lifetime to the carrier lifetime in the active (passive) material, μ is the pump parameter of the active material, γ is the absorption parameter of the passive material, s is the saturation parameter, and B is the coefficient of radiative recombination. For more details on the definition of the parameters, see Ref. [12]. Notice, however, that in the definitions of μ and γ the inclusion of quadratic recombination implies that the coefficients η_1 and η_2 must be replaced by $\eta_1(1 - B\eta_1)$ and $\eta_2(1 - B\eta_2)$. Therefore, if the absorber is not pumped, $\gamma = \eta_2(1 - B\eta_2)$.

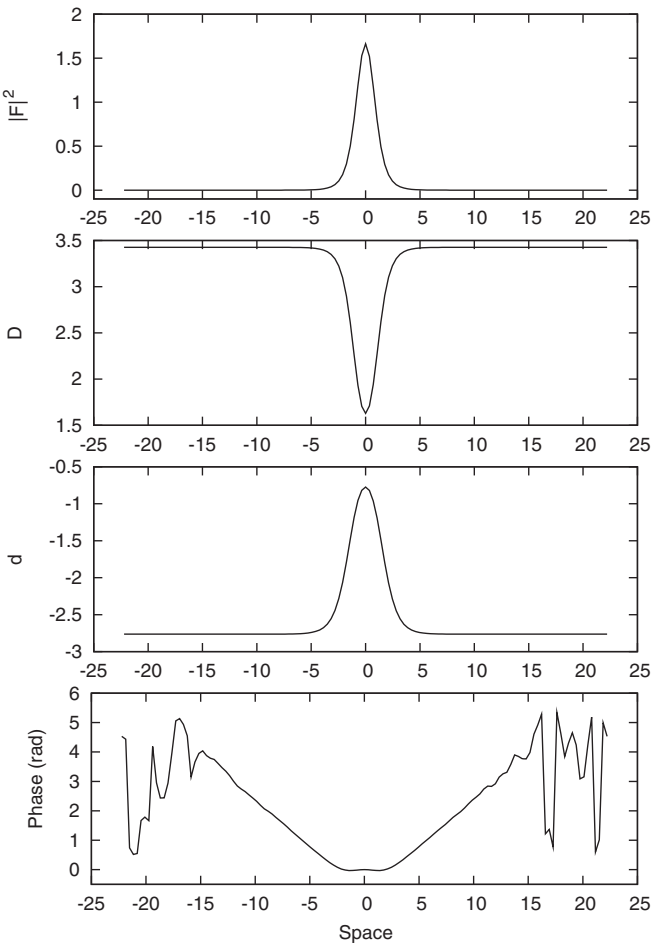

FIG. 2. Profiles of the field intensity, of the populations D and d, and of the field phase for the CS at $\mu = 4.6$.

For the choice of parameters $s = 1$, $\gamma = 2$, $B = 0.1$, $\alpha = 2$, $\beta = 1$, and $b_1 = b_2 = 0.003$, the homogeneous stationary solution and the stable CS branch are shown in Fig. 1 as a function of the pump parameter μ. The off solution is stable below the laser threshold $\mu_{\text{thr}} \simeq 5.18$ and is unstable above it. The nontrivial homogeneous solution is unstable everywhere due to the diffraction term. The stability range of the CS is very sensitive to the ratio $r = b_2/b_1$ of the two decay rates of the population variables. For $r = 1$, the CSs are stable in the interval $4.56 < \mu < 5.15$. In this paper, we focus on $\mu = 4.6$ because, for that pump value, the CS can easily be switched on and off incoherently as shown in Ref. [14].

Since we are interested in the interaction of two CSs, it is important to know the size of a CS in the different physical variables. The profiles of the field intensity, of the two populations D and d, and of the field phase for the CS at $\mu = 4.6$ are shown in Fig. 2. The size of the CS in the two population profiles is slightly larger than in the field intensity, but the most striking feature is that the coherence area of the CS, i.e., the region where the field has a definite phase, is much

broader. We then expect long-range interactions between two CSs mediated by the phase [27].

In Fig. 2, the horizontal axis is one adimensional transverse coordinate. In order to estimate the real value of one spatial unit, we can compare the FWHM (in the field intensity) of the CS from the numerical simulations with the experimental ones. The FWHM is about two space units in the numerical simulations, and it ranges from 10 [4,9] to 12 μm [11] in the experiments. Hence, one space unit in the numerical simulation corresponds to about 5 to 6 μm. This must be kept in mind when we want to obtain physical values of the distance between the CSs from the numerical simulations.

From Figs. 6 and 7 of Ref. [9], it also is possible to evaluate the actual size of the CS phase profile by looking at the spatial area in the far field that is characterized by interference fringes: Even if it is difficult to quantify it, one can estimate that the phase profile is three to four times larger than the intensity profile. The fact that, in our case, it is even larger can be attributed to spatial disorder that limits the spatial coherence of the CS in the experiment.

III. NUMERICAL SIMULATIONS

The dynamical equations were integrated numerically using a split-step method with periodic boundary conditions. We used a 128×128 grid with a space step $ds = 0.25$, which, according to the above discussion, corresponds to 1.25–1.5 μm. The time unit is the photon lifetime, which is typically on the order of a few picoseconds. The effects of spontaneous emission noise are simulated adding stochastic terms in the form of Gaussian white-noise sources with zero mean and unit variance, uncorrelated both in time and in space, to Eq. (1).

In order to incoherently switch the CS on and off, we superimposed to the homogeneous pump a Gaussian pulse of the form

$$\mu(x,y) = \mu_0 + \eta e^{[-(x-x_0)^2-(y-y_0)^2]/w^2}, \tag{5}$$

which simulates the injection of a Gaussian current pulse of amplitude η and width w, centered in the point (x_0, y_0) for a certain injection time t_{inj}. The injection parameters that we used to create a CS are $\eta = 4.6$, $w = 2\sqrt{2}$, and $t_{\mathrm{inj}} = 300$. As shown in Ref. [14], to switch off the CS, narrower and more intense beams must be used. Thus, we increased the amplitude to $\eta = 20$, reduced the width to $w = 1.2$, and reduced the injection time to $t_{\mathrm{inj}} = 100$.

Figure 3 shows the dynamics of the field intensity during switch on and switch off. The switch-on dynamics resembles that of a class-B laser, which is suddenly brought above threshold: large damped pulses in the initial stage and damped harmonic oscillations in the final stage. For what follows, it is important that, immediately after the end of the injection, the intensity falls to almost zero, and it remains very low for some tens of time units. The switch-off process is much faster because the CS simply disappears as soon as the associated hole in the active population is filled by the injected carriers.

In the following, as initial condition of our numerical simulation, we took a CS placed in the position (40,40) of the grid and tried to create a new CS by injecting a switch-on beam centered in the position $(40 + N, 40 + N)$. Hence, both

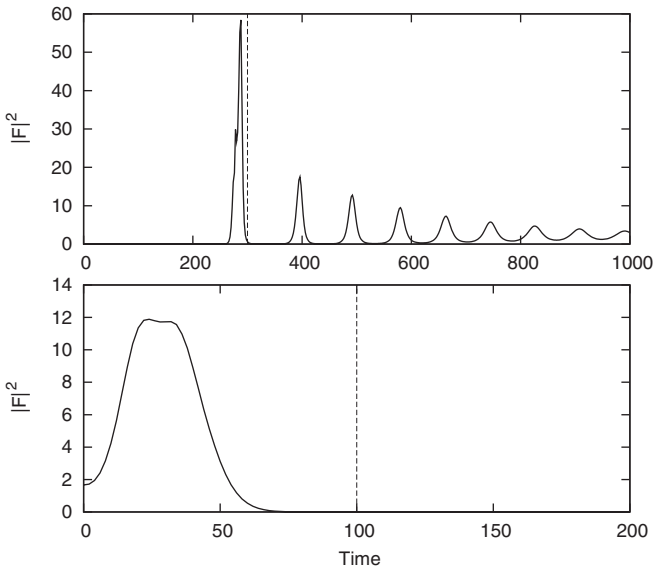

FIG. 3. Field intensity dynamics when a CS is switched on (upper panel) and off (lower panel) by injection of carriers in the active material. In both figures, the vertical dashed lines denote the time at which injection ceases.

CSs are on the diagonal of the square, and their initial distance is $\Delta = \sqrt{2}N\,ds$. We observed different behaviors as N varied.

The results can be classified in three groups: $16 \leqslant N \leqslant 26$ (small distance), $27 \leqslant N \leqslant 36$ (medium distance), and $N \geqslant 37$ (large distance). For $N \leqslant 15$, the situation is less clear. In some cases, we find results similar to those obtained for larger N because the injected beam repels the existing CS so that, at the end, the distance of the two CSs is much larger than Δ. In other cases, the injected beam switches off the existing CS without creating a new one, and the laser ends in the off state.

A. Small distance

For $16 \leqslant N \leqslant 26$ ($5.66 \leqslant \Delta \leqslant 9.19$), the attempt to create a second CS fails. For those relatively small distances, the switch-on process of a new CS perturbs the existing one. In particular, when the giant pulse that is formed in the injection point falls to zero at the end of the injection, the intensity of the existing CS also is strongly reduced. Hence, at the end of the injection, the field intensity is very low everywhere, although there are two dips in the carriers centered in the grid points (40,40) and $(40 + N, 40 + N)$.

Typical profiles of the field intensity and of the active population D at the end of the injection are shown in Fig. 4 for $N = 21$. At this point, the possible outcomes are three: (i) only the old CS recovers and survives, (ii) only the new CS recovers and survives, and (iii) both CSs recover and compete, but at the end, only one survives.

The last behavior has been found for $N = 18, 19, 20$, and we show the results of the simulations for $N = 18$ in Fig. 5. The two CSs exhibit strong intensity oscillations that last for a relatively long time, on the order of 10^6 time units, i.e., a few microseconds. Yet, in all three cases, one of the two CSs switches off suddenly and unpredictably, leaving the other one alone.

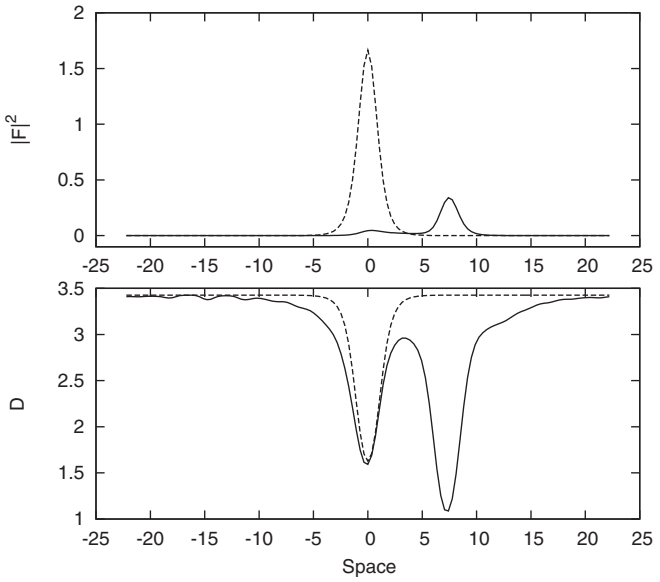

FIG. 4. Profiles of the field intensity (upper figure) and of the active population D along one diagonal of the integration square at the beginning (dashed line) and at the end (solid line) of the injection for $N = 21$.

We have analyzed the dynamics of the two oscillating CSs, considering various temporal sequences extracted from the complete evolution. The motion of intensities I_1 and I_2 and phases θ_1 and θ_2, calculated at the peaks of the two CSs over 10 000 time units, are shown in Figs. 5(a) and 5(b). Both the intensity and the phase plots look uncorrelated. To quantify

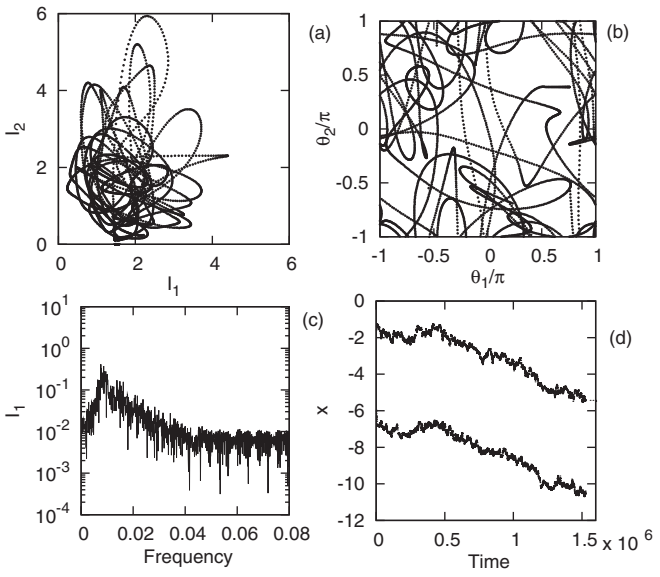

FIG. 5. Two oscillating CSs for $N = 18$. Plots of the (a) intensities I_1 and I_2, (b) phases θ_1 and θ_2 at the peaks of the two CSs, (c) power spectrum of I_1 calculated over a window of 10 000 time units, and (d) time evolution of the horizontal coordinate for the whole duration of the interaction. At about $t = 1.5 \times 10^6$ the leftmost CS disappears.

the degree of correlation, we have used the cross-correlation function defined as

$$C(\tau) = \frac{\langle \Delta I_1(t+\tau)\Delta I_2(t)\rangle}{\sqrt{\langle \Delta I_1(t)^2\rangle \langle \Delta I_2(t)^2\rangle}}, \tag{6}$$

where ΔI_1 and ΔI_2 are the deviations in the intensity of the two CSs with respect to their time-averaged values. The cross-correlation function is 1 for perfect correlation, -1 for perfect anticorrelation, and 0 for no correlation. We always have found values smaller in absolute value than 0.3, indicating a low degree of correlation.

Figure 5(c) shows the power spectrum of I_1; the one for I_2 is very similar. The spectrum displays a maximum at a frequency close to the relaxation oscillation frequency, which is given approximately by $\sqrt{b_{1,2}}/2\pi \simeq 8.7 \times 10^{-3}$. For higher frequencies, we have the $1/f$ behavior typical of chaotic dynamics.

As long as both CSs are present, they move randomly along the straight line connecting them, i.e., the square diagonal. The time evolution of the horizontal coordinate of the two CSs, which is equal to the vertical one, is shown in Fig. 5(d). During this motion, the distance remains more or less constant, which means that the two CSs do not merge into one as in Ref. [19]. On the contrary, one of the two collapses.

B. Medium distance

For $27 \leqslant N \leqslant 36$ ($9.55 < \Delta < 12.73$), a new CS can be created without destroying the preexisting one. The two main features of the CS pairs are as follows: (i) their distance can assume only two definite values, and (ii) they display partial out-of-phase locking, as will be explained, accompanied by small oscillations in the peak intensity.

The two possible values of the distance are 10.95 and 11.97, which are the final values obtained for $27 \leqslant N \leqslant 32$ ($9.55 \leqslant \Delta \leqslant 11.31$) and for $33 \leqslant N \leqslant 36$ ($11.67 \leqslant \Delta \leqslant 12.73$), respectively. The time evolution of the distance of the two CSs toward the two different final values is shown in Fig. 6. The irregularities visible in the curves are due to the finiteness of the space step that prevents us from following with continuity the position of the peak of the CS. The two CSs experience repulsive or attractive forces depending on their initial distance.

For the smaller initial distances ($N = 27,28$), the relative phase of the two CSs, i.e., the difference in the phases at the peaks, initially locks at π as the two CSs move rapidly away, one from the other, but when the CSs are sufficiently far apart, their phases unlock, as shown in Fig. 7 for $N = 27$. The relative phase displays bounded oscillations around π, which means that the two phases still are partially locked. In all the other cases, the relative phase oscillates around π from the beginning.

Figure 8 show the plots of intensities I_1 and I_2 and phases θ_1 and θ_2 for the two bound states at distances 10.95 (left column) and 11.97 (right column).

First, let us consider the phase motion. If phases θ_1 and θ_2 were locked at π, the phase plots would be the straight lines of slope 1 shown by the dashed lines. In our case, the two phases advance in time at different velocities so that the trajectory is different from a straight line. Yet, after one period, both phases

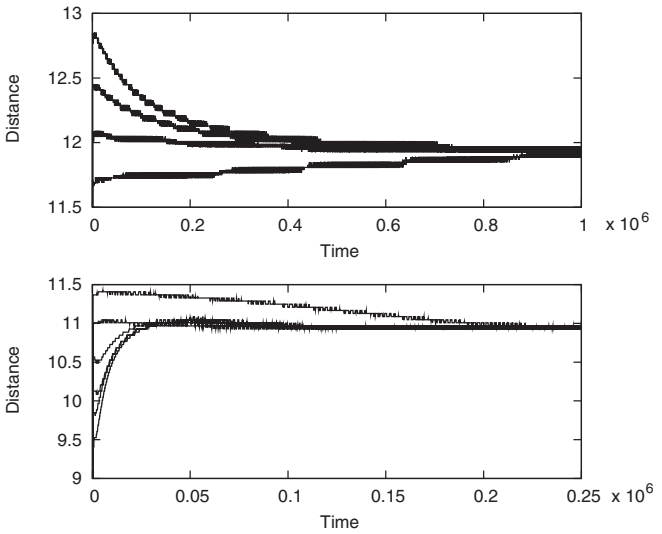

FIG. 6. Time evolution of the distance for different values of the distance of the injected beam from the existing CS. Moving upward, N increases by 1 from 27 to 32 in the bottom figure and from 33 to 36 in the top figure.

have advanced by 2π, and then the trajectory repeats itself if the phases are calculated mod 2π.

This is a behavior typical of biological systems, which is called phase entrainment [28], and it has been demonstrated to play an important role in heart diseases [29]. In nonlinear optics, phase entrainment was found in solid-state laser arrays [30], in a laser with optical injection [31], and, much more recently, between two laser modes coupled by feedback [32]. Strictly speaking, however, phase entrainment is a kind of partial locking of two oscillators with different proper frequencies. In our case, instead, the two CSs are identical and, if alone, they would have the same carrier frequency.

The period of phase oscillations is much larger than that of the relaxation oscillations ($\sim$100 time units) and increases with the distance. It is 2078.5 time units for the CSs at distance 10.95 and 3378 time units for the CSs at distance 11.97.

To understand the intensity plots, we must consider that, unlike in conventional lasers, in a CSL frequency and intensity of the CS are not independent of each other. Since, in a partially phase-locked state, the frequency of each CS is slightly modulated in time, this modulation necessarily is

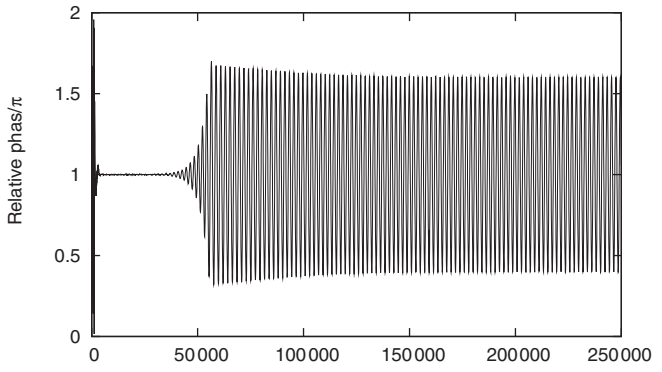

FIG. 7. Time evolution of the relative phase of the two CSs for $N = 27$.

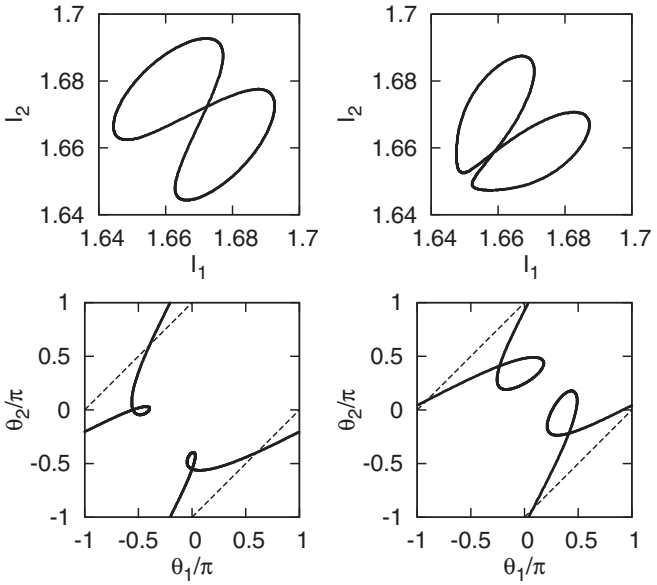

FIG. 8. Plots of intensities I_1 and I_2 and phases θ_1 and θ_2 at the peaks of the two CSs when the final distance is about 11 (left column) and about 12 (right column). In the plots for the phases, the dashed lines represent the situation of perfect out-of-phase locking (phase difference equal to π). In these simulations, the noise term was set equal to zero to better appreciate the deterministic dynamics.

accompanied by small correlated oscillations in the intensities of the CS, which produce the closed trajectories shown in the upper row of Fig. 8.

In all the above cases, the two CSs, although correlated, can be switched off independently with the same beam used to switch off the single CS.

It is worth noting that the existence of two preferred distances for CSs to form molecules cannot be attributed to tails in the intensity profile of the CS as in externally driven passive cavities [20] because, in our system, the CS profile does not exhibit tails in any variable (see Fig. 2).

C. Large distance

For $N \geqslant 37$ ($\Delta \geqslant 13.08$), the two CSs lock very soon at the same phase, and they start moving apart. This behavior resembles that of the solitons in the complex quintic Ginzburg-Landau equations with large spectral filtering [33].

The solitons repel each other until their distance is about 21 to 22 space units, which is more than ten times the FWHM of the soliton intensity profile. Long-range interactions, up to ten soliton diameters, were found in optical solitons propagating in materials exhibiting optical thermal nonlinearities, for which the interaction was mediated by heat transfer [34]. But in our case, thermal effects are neglected, and the interaction at such a large distance cannot even be attributed to the charge carriers because the final distance also is equal to several soliton diameters in the population variables.

Thus, the only explanation is that the coherence domain associated with a CS is much more extended than its intensity FWHM as shown in Fig. 2.

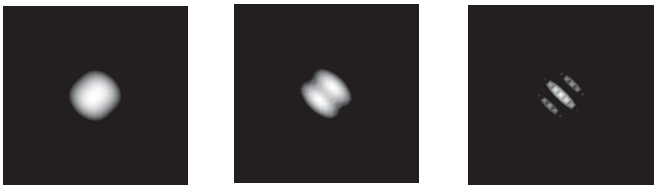

FIG. 9. Time average of the far-field intensity distribution of the two CSs for $N = 18$ (left), $N = 30$ (center), and $N = 37$ (right).

IV. DISCUSSION AND CONCLUSIONS

Our numerical simulations have demonstrated that a pair of CSs in a VCSEL with a saturable absorber interact in three different ways depending on their distances. For small distances ($16 \leqslant N \leqslant 26$), only one of the two CSs survives, and in the transient evolution, they may exhibit strong uncorrelated oscillations. For medium distances ($27 \leqslant N \leqslant 36$), the two CSs arrange their position to form a bound state at two possible fixed distances, while their intensities display small amplitude correlated oscillations, and the relative phase slowly oscillates around π. Finally, for large distances ($N \geqslant 37$), the two CSs lock in phase, and they move apart, one from the other, until they reach a distance larger than ten soliton diameters at which they do not feel each other.

These three different behaviors lead to different far-field patterns as shown in Fig. 9 where we consider values of N representative of the three behaviors: for $N = 18$, the absence of correlation produces a single lobe in the far field, for $N = 30$, the partial phase locking around π manifests itself in two bright fringes, and for $N = 37$, we have the typical interference pattern produced by two in-phase sources. We can note that, for the case of partial phase locking ($N = 30$), the contrast is reduced because the interference fringes slowly move across a fixed position.

We can compare these results with some recent experimental findings. Mutual coherence of CSs in a VCSEL with a saturable absorber in the face-to-face configuration was investigated in Ref. [9], analyzing the interference patterns. It was shown that two CSs well separated in space, i.e., with a region of zero intensity in between, always are unlocked. Yet, a possible explanation was that the two CSs had different frequencies associated with different longitudinal modes because the face-to-face configuration allowed for the oscillations of several longitudinal modes. The same happens in the VCSEL with frequency-selective feedback [4].

Hence, the best candidate for the observation of phase locking of two CSs is the monolithic VCSEL with a saturable absorber because the shortness of the cavity ensures that only one longitudinal mode can be active. In Ref. [11], however, the question of the mutual coherence of two CSs has not been investigated. Instead, it has been shown that the minimal distance at which two CSs can exist as separated entities is 28 μm. If we assume, in agreement with Ref. [11], that one spatial unit in our simulations corresponds to 6 μm, we must conclude that two CSs cannot survive until their distance is smaller than about 55 μm and that, in the two states that are partially phase locked around π, the distances of the two CSs are 66 and 72 μm, respectively. Hence, the minimum distance is more than twice as large as in Ref. [11]. A possible explanation is that our result has been obtained with a particular set of parameters, and we cannot exclude that the equilibrium distances depend strongly on some parameter. Another reason may lie in the presence of defects and roughness in the material and cavity [35–37], which may pin the CS to preferred positions, even if, in an ideal world, they would prefer to stay far apart from each other. For the same reason, a weak phase coupling, as in the case of large distances (where two CSs lock in phase), could completely be screened by inhomogeneities effects.

Moving from optics to fluid dynamics, the existence of bound states at discrete distances also was demonstrated for droplets bouncing on the surface of a vibrated liquid. In that case, the distances were shifted multiples of the wavelength of the surface waves [38].

This is not the only aspect that makes CSs similar to bouncing droplets. Analogies also were found in the motion of self-propelled CSs and droplets (walkers) inside a square domain [39–41].

ACKNOWLEDGMENTS

G.T. and F.P. thank S. Barland for useful discussions. G.T., F.P., and L.A.L. acknowledge support from the Italian Ministry of Research (MIUR) through the Futuro in Ricerca FIRB Grant No. PHOCOS-RBFR08E7VA.

[1] T. Ackemann, W. Firth, and G.-L. Oppo, Adv. At., Mol., Opt. Phys. **57**, 323 (2009).

[2] S. Barland, J. R. Tredicce, M. Brambilla, L. A. Lugiato, S. Balle, M. Giudici, T. Maggipinto, L. Spinelli, G. Tissoni, T. Knödl, M. Miller, and R. Jäger, Nature (London) **419**, 699 (2002).

[3] X. Hachair, F. Pedaci, E. Caboche, S. Barland, M. Giudici, J. R. Tredicce, F. Prati, G. Tissoni, R. Kheradmand, L. A. Lugiato, I. Protsenko, and M. Brambilla, IEEE J. Sel. Top. Quantum Electron. **12**, 339 (2006).

[4] Y. Tanguy, T. Ackemann, W. J. Firth, and R. Jäger, Phys. Rev. Lett. **100**, 013907 (2008).

[5] A. J. Scroggie, W. J. Firth, and G.-L. Oppo, Phys. Rev. A **80**, 013829 (2009).

[6] N. Radwell and T. Ackemann, J. Quantum Electron. **45**, 1388 (2009).

[7] P. Genevet, S. Barland, M. Giudici, and J. R. Tredicce, Phys. Rev. Lett. **101**, 123905 (2008).

[8] P. Genevet, L. Columbo, S. Barland, M. Giudici, L. Gil, and J. R. Tredicce, Phys. Rev. A **81**, 053839 (2010).

[9] P. Genevet, M. Turconi, S. Barland, M. Giudici, and J. R. Tredicce, Eur. Phys. J. D **59**, 109 (2010).

[10] T. Elsass, K. Gauthron, G. Beaudoin, I. Sagnes, R. Kuszelewicz, and S. Barbay, Appl. Phys. B **98**, 327 (2010).

[11] T. Elsass, K. Gauthron, G. Beaudoin, I. Sagnes, R. Kuszelewicz, and S. Barbay, Eur. Phys. J. D **59**, 91 (2010).

[12] M. Bache, F. Prati, G. Tissoni, R. Kheradmand, L. A. Lugiato, I. Protsenko, and M. Brambilla, Appl. Phys. B **81**, 913 (2005).
[13] F. Prati, P. Caccia, G. Tissoni, L. A. Lugiato, K. M. Aghdami, and H. Tajalli, Appl. Phys. B **88**, 405 (2007).
[14] K. Mahmoud Aghdami, F. Prati, P. Caccia, G. Tissoni, L. A. Lugiato, R. Kheradmand, and H. Tajalli, Eur. Phys. J. D **47**, 447 (2008).
[15] F. Prati, G. Tissoni, L. A. Lugiato, K. Mahmoud Aghdami, and M. Brambilla, Eur. Phys. J. D **59**, 73 (2010).
[16] N. N. Rozanov and S. V. Fedorov, Opt. Spektrosk. **72**, 1394 (1992) [Opt. Spectrosc. **72**, 782 (1992)].
[17] S. V. Fedorov, A. G. Vladimirov, G. V. Khodova, and N. N. Rosanov, Phys. Rev. E **61**, 5814 (2000).
[18] M. Brambilla, L. A. Lugiato, and M. Stefani, Europhys. Lett. **34**, 109 (1996).
[19] L. Spinelli, G. Tissoni, M. Brambilla, F. Prati, and L. A. Lugiato, Phys. Rev. A **58**, 2542 (1998).
[20] A. G. Vladimirov, J. M. McSloy, D. V. Skryabin, and W. J. Firth, Phys. Rev. E **65**, 046606 (2002).
[21] G. I. Stegeman and M. Segev, Science **286**, 1518 (1999).
[22] H. G. Winful and S. S. Wang, Appl. Phys. Lett. **53**, 1894 (1988).
[23] F. Prati, D. Vecchione, and G. Vendramin, Opt. Lett. **22**, 1633 (1997).
[24] N. N. Rosanov, S. V. Fedorov, and A. N. Shatsev, Quantum Electron. **38**, 41 (2008).
[25] N. N. Rosanov, S. V. Fedorov, and A. N. Shatsev, Appl. Phys. B **81**, 937 (2005).
[26] S. V. Fedorov, N. N. Rosanov, and A. N. Shatsev, Opt. Spectrosc. **102**, 449 (2007).
[27] L. Columbo, L. Gil. and J. Tredicce, Opt. Lett. **33**, 995 (2008).
[28] T. Chakraborty and R. H. Rand, Int. J. Non-Linear Mech. **23**, 369 (1988).
[29] W. L. Keith and R. H. Rand, J. Math. Biol. **20**, 133 (1984).
[30] Y. Braiman, T. A. B. Kennedy, K. Wiesenfeld, and A. Khibnik, Phys. Rev. A **52**, 1500 (1995).
[31] P. A. Braza and T. Erneux, Phys. Rev. A **41**, 6470 (1990).
[32] J. Thevenin, M. Romanelli, M. Vallet, M. Brunel, and T. Erneux, Phys. Rev. Lett. **107**, 104101 (2011).
[33] V. V. Afanasjev and N. Akhmediev, Phys. Rev. E **53**, 6471 (1996).
[34] C. Rotschild, B. Alfassi, O. Cohen, and M. Segev, Nat. Phys. **2**, 769 (2006).
[35] F. Pedaci, G. Tissoni, S. Barland, M. Giudici, and J. Tredicce, Appl. Phys. Lett. **93**, 111104 (2008).
[36] E. Caboche, F. Pedaci, P. Genevet, S. Barland, M. Giudici, J. Tredicce, G. Tissoni, and L. A. Lugiato, Phys. Rev. Lett. **102**, 163901 (2009).
[37] E. Caboche, S. Barland, M. Giudici, J. R. Tredicce, G. Tissoni, and L. A. Lugiato, Phys. Rev. A **80**, 053814 (2009).
[38] A. Eddi, A. Decelle, E. Fort, and Y. Couder, Europhys. Lett. **87**, 56002 (2009).
[39] S. Protiére, A. Boudaoud, and Y. Couder, J. Fluid Mech. **554**, 85 (2006).
[40] A. Eddi, E. Fort, F. Moisy, and Y. Couder, Phys. Rev. Lett. **102**, 240401 (2009).
[41] F. Prati, L. A. Lugiato, G. Tissoni, and M. Brambilla, Phys. Rev. A **84**, 053852 (2011).